THE JOURNAL OF PHYSICAL CHEMISTRY LETTERS
A JOURNAL OF THE AMERICAN CHEMICAL SOCIETY

pubs.acs.org/JPCL Letter

Revealing Local Disorder in a Silver-Bismuth Halide Perovskite upon Compression

Samuel P. Girdzis, Yu Lin,* Linn Leppert, Adam H. Slavney, Sulgiye Park, Karena W. Chapman, Hemamala I. Karunadasa, and Wendy L. Mao*

Cite This: *J. Phys. Chem. Lett.* 2021, 12, 532−536 Read Online

ACCESS | Metrics & More | Article Recommendations | Supporting Information

ABSTRACT: The halide double perovskite $Cs_2AgBiBr_6$ has emerged as a promising nontoxic alternative to the lead halide perovskites $APbX_3$ (A = organic cation or Cs; X = I or Br). Here, we perform high-pressure synchrotron X-ray total scattering on $Cs_2AgBiBr_6$ and discover local disorder that is hidden from conventional Bragg analysis. While our powder diffraction data show that the average structure remains cubic up to 2.1 GPa, analysis of the X-ray pair distribution function reveals that the local structure is better described by a monoclinic space group, with significant distortion within the Ag−Br and Bi−Br octahedra and off-centering of the Cs atoms. By tracking the distribution of interatomic Cs−Br distances, we find that the local disorder is enhanced upon compression, and we corroborate these results with molecular dynamics simulations. The observed local disorder affords new understanding of this promising material and potentially offers a new parameter to tune in halide perovskite lattices.

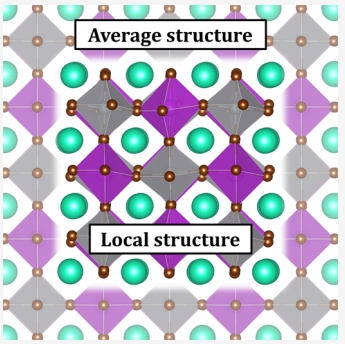

Halide perovskites have attracted extraordinary interest for photovoltaic applications, due to their low-cost solution-state syntheses, long carrier lifetimes, and vast possibilities for compositional tuning.[1,2] Power conversion efficiencies of perovskite-based devices have climbed rapidly from less than 4% initially[3] to over 25% last year.[4] The all-inorganic double perovskite $Cs_2AgBiBr_6$[5,6] aims to address the toxicity and stability challenges of the more prominent hybrid lead halide perovskites. $Cs_2AgBiBr_6$ has a reasonable band gap of 1.95 eV and is far more stable to heat and humidity than $(MA)PbI_3$ and $(MA)PbBr_3$ (MA = methylammonium).[5] However, its indirect bandgap results in weak visible-light absorption. Using compression, it is possible to directly alter the structures of halide perovskites, which in turn allows for tuning of optoelectronic properties.[7−15] In a previous study, $Cs_2AgBiBr_6$ exhibited band gap narrowing with compression to ca. 3 GPa, which was attributed to contraction of the Ag−Br and Bi−Br octahedra while cubic symmetry was maintained.[16] However, that study only described the evolution of the average structure of $Cs_2AgBiBr_6$. Understanding the local structure of $Cs_2AgBiBr_6$ under compression has the potential to further illuminate the photophysics of this material and its analogs. Indeed, most elpasolites, like $Cs_2AgBiBr_6$, have cubic $Fm\bar{3}m$ symmetry at ambient conditions with no apparent octahedral tilting or distortions, although their 2-D derivatives show considerable inter- and intraoctahedral distortions.[17] Local structural disorder has a significant influence on the optoelectronic properties of halide perovskites. Spontaneous octahedral tilting in the cubic phases of $CsMX_3$ (M = Pb, Sn; X = I, Br, Cl, F) halide perovskites leads to increases in their band gaps due to decreased overlap of the M *s* and X *p* orbitals that contribute to the valence band.[18] Furthermore, calculations have shown that local asymmetry combined with spin−orbit coupling produces a spin-split band gap in the related inorganic halide perovskite $CsPbI_3$, leading to an indirect rather than direct band gap.[19] In $Cs_2AgBiBr_6$ itself, the large Stokes shift and broad width of its photoluminescence emission have been attributed to strong electron−phonon coupling via the Frohlich interaction; however, calculations based on the cubic structure predicted coupling of only moderate strength, with local structural disorder being a possible explanation for this mismatch.[20] Existing studies on local structural disorder in halide perovskites are limited to ABX_3[18,19,21,22] and $A_2B\square X_6$[23,24] compositions, where □ is a vacancy, and we are not aware of high-pressure studies of such disorder.

To better understand possible local structural disorder in $Cs_2AgBiBr_6$, we conducted high-pressure synchrotron X-ray total scattering, as typical powder or single-crystal X-ray diffraction (XRD) based on Bragg peaks is limited to observing the average crystalline structure. Analysis of the atomic pair distribution function (PDF) reveals that the average $Fm\bar{3}m$ model[5] poorly describes the material's structure at the length scale of a single unit cell. We propose a lower-symmetry model

Received: November 16, 2020
Accepted: December 22, 2020

https://dx.doi.org/10.1021/acs.jpclett.0c03412
J. Phys. Chem. Lett. 2021, 12, 532−536

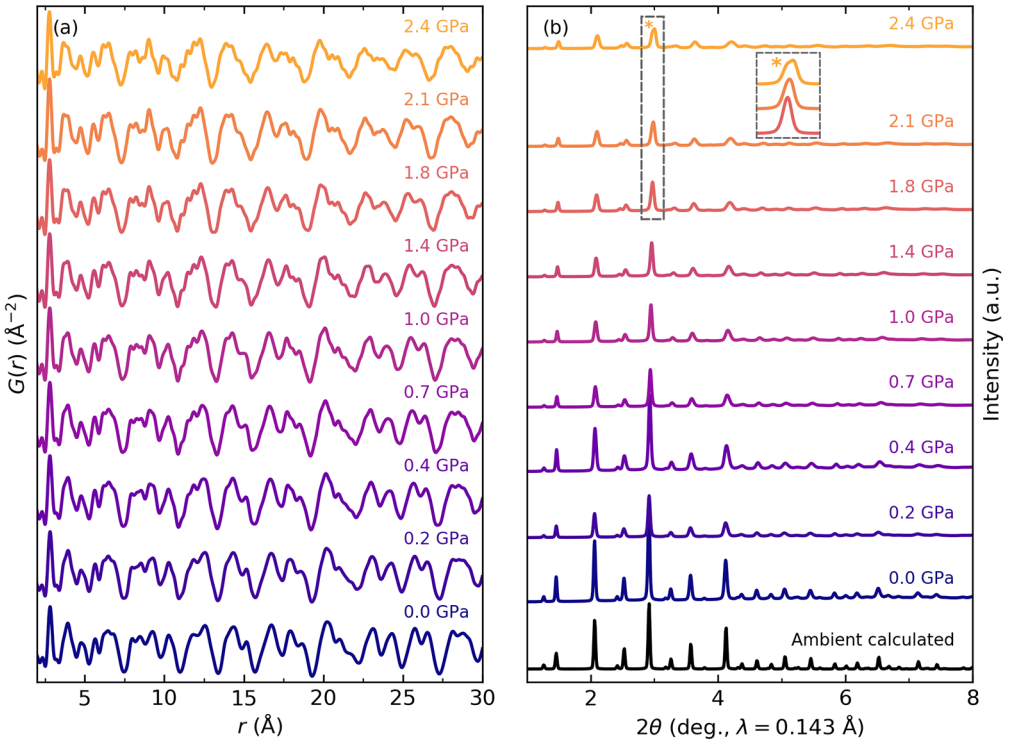

Figure 1. (a) Experimental X-ray PDF data of $Cs_2AgBiBr_6$. (b) Experimental powder XRD data, collected concurrently with PDF data. Also shown is a pattern calculated from the $Fm\bar{3}m$ model of Slavney et al.[5] Inset shows splitting of the cubic (400) peak at 2.4 GPa (marked *).

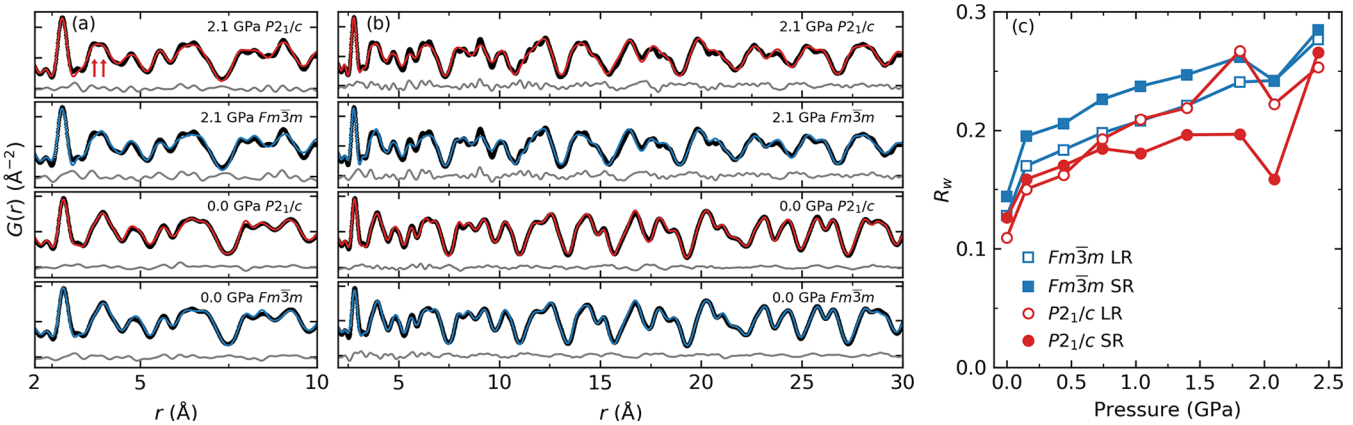

Figure 2. (a) Fits of the X-ray PDFs at short range (SR, 2−10 Å) with space groups $P2_1/c$ and $Fm\bar{3}m$ at selected pressures. The lower-symmetry space group $P2_1/c$ is necessary to capture the broad second nearest-neighbor peak at 2.1 GPa, marked with arrows. (b) Fits of the X-ray PDFs at long range (LR, 2−30 Å). Both space groups perform similarly in modeling the PDF at longer distances. (c) Comparison of R_w values for the two space groups and two fit ranges with compression.

with space group $P2_1/c$ to describe local tilting between and distortion within the Ag−Br and Bi−Br octahedra and also off-centering of the Cs atoms, and we corroborate this model with molecular dynamics (MD) simulations. Our results agree with halide disorder observed in related single B-site halide perovskites, both experimentally[21,22] and theoretically,[18,25,26] and potentially support the unexpectedly large electron−phonon interaction in $Cs_2AgBiBr_6$ described above.[20]

The $Cs_2AgBiBr_6$ sample was synthesized according to our previous method,[5] with an additional step of ball milling to ensure good powder averaging. The sample was loaded in a diamond anvil cell, and high-pressure X-ray total scattering data were collected at beamline 11-ID-B at the Advanced Photon Source at Argonne National Laboratory using an energy of 86.7 keV (0.143 Å). The 2-D scattering patterns were masked to remove diamond reflections and integrated using the Fit2D software package.[27] The PDFgetX2 software program[28] was used to extract the structure factor $S(Q)$ up to $Q = 18$ Å^{-1}, which was then transformed to the real-space PDF $G(r)$ (Figure 1a). We collected powder XRD data at a longer sample-to-detector distance for average structure analysis (Figure 1b).

The PDFs were analyzed using the PDFgui program,[29] allowing us to refine various structural models to account for local disorder as well as pressure-induced changes. Our first-principles MD calculations were performed using a canonical (NVT) ensemble with a Nosé−Hoover thermostat, as implemented in the VASP[30,31] code, with the exchange-

https://dx.doi.org/10.1021/acs.jpclett.0c03412
J. Phys. Chem. Lett. 2021, 12, 532−536

correlation approximation PBEsol.[32] The total runtime of each simulation was 40 ps, and we allowed for an equilibration time of 1.2 ps. Structures were visualized using the VESTA program.[33] Further experimental and computational details are in the Supporting Information.

The ambient-pressure structure with space group $Fm\bar{3}m$ was the starting point for our analysis. We fit the PDF series over two ranges, i.e., 2−10 Å (short range, SR, Figure 2a) and 2−30 Å (long-range, LR, Figure 2b). The full pressure series of fits are shown in Figures S1−S4. The figure of merit R_w was used to compare the fitted model and the experimental data, with lower values indicating better agreement. The cubic model performs significantly worse at short range compared to long range and generally becomes worse for both ranges as pressure increases (Figure 2c). The $Fm\bar{3}m$ fits yielded highly anisotropic thermal parameters for the Br atoms, in agreement with behavior observed in related halide perovskites.[21,22,26] The 2.4 GPa data have poor R_w values due to the onset of a transition to a high-pressure tetragonal phase, evident from the split (400) diffraction peak at $2\theta \approx 3°$ (Figure 1b inset). At pressures of 2.1 GPa and below, the powder XRD data reflect an $Fm\bar{3}m$ structure as no split or emergent peaks were observed.

However, the cubic model was unable to account for how the second nearest-neighbor PDF peak at ca. 4 Å broadens with pressure (Figure 2a). To describe the local structure upon compression, we obtained the best results by starting with the low-temperature phase of the related halide perovskite $CsSnBr_3$, which has space group *Pnma* and $a^-b^+a^-$ tilts in Glazer notation.[21,34] Importantly, low-temperature $CsSnBr_3$ exhibited a split second nearest-neighbor peak in its X-ray PDF. We adapted this structure by matching the lattice parameters pressure-by-pressure to values from our long-range cubic PDF fits of $Cs_2AgBiBr_6$, which were in good agreement with values obtained by synchrotron powder XRD, and by substituting the Sn atoms with a rock salt-ordered arrangement of Ag and Bi atoms. Due to the existence of two different, ordered B-site atoms in an $a^-b^+a^-$ tilt system, the space group is reduced to $P2_1/c$.[35]

The $P2_1/c$ model fits the short-range PDFs significantly better at higher pressures (Figures 2a and 2c). Notably, the $P2_1/c$ model simulates the broad second nearest-neighbor peak, corresponding to Cs−Br and Br−Br atomic pairs. Moreover, this model can still describe the structure at long range over the range of experimental pressures (Figures 2b and 2c). This indicates the presence of local disorder which is hidden from observation by conventional XRD. The local distortions of the Br octahedral network in the $P2_1/c$ model explain the highly anisotropic Br thermal parameters when the structure is considered from the average, $Fm\bar{3}m$ perspective. In fact, this anisotropy increases with pressure (Figure S5). Also, we find that the $P2_1/c$ fits include Cs migration from its high-symmetry sites. Considering the Cs−Br interatomic distances, which are all equal in the $Fm\bar{3}m$ model, we see that the distribution broadens as pressure increases and consistently is broader at short range than at long range (Figure S6); that is, the local disorder is enhanced upon compression.

To better understand the effect of Br distortion and Cs off-centering on the PDF, we compare four models for the PDF at 2.1 GPa. Figure 3a shows the $P2_1/c$ fit at short range, which provides the best fit of the local structure. Figures 3b and 3c show calculated PDFs with only Br distortion and only Cs-off centering, respectively. Lastly, Figure 3d shows the $Fm\bar{3}m$ long-range fit over 2−10 Å, which is very similar to the $Fm\bar{3}m$ short-range fit (Figure 2a). From this comparison, it is clear that both Cs off-centering and Br distortion are necessary to describe the local structure upon compression. This agrees with recent theoretical work on related $CsMX_3$ (M = Pb, Sn; X = I, Br) halide perovskites which found that the cubic and tetragonal phases are dynamically unstable with respect to the orthorhombic ground state, and this orthorhombic $b^-b^-a^+$ tilted arrangement, analogous to $P2_1/c$ in our case, is stabilized by Cs off-centering.[25]

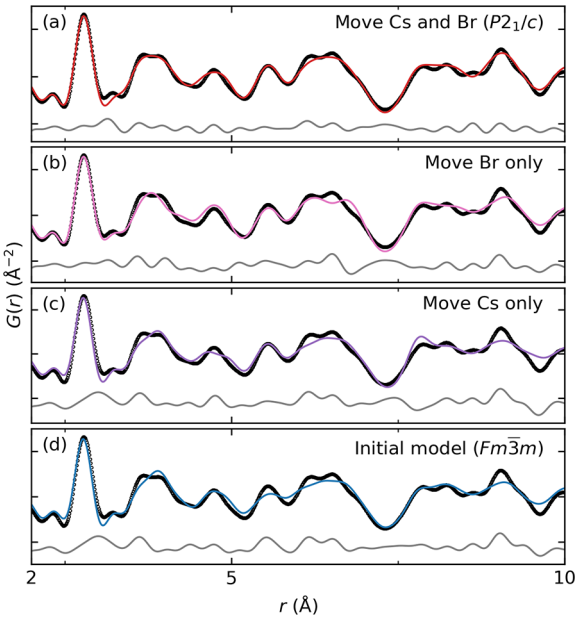

Figure 3. Comparison of the effects of Br distortion and Cs off-centering at 2.1 GPa. (a) PDF fit using the $P2_1/c$ model, allowing both Cs off-centering and Br distortion. (b) Calculated PDF with Br distortion while Cs remains on high-symmetry sites. (c) Calculated PDF with Cs off-centering while Br remains on high-symmetry sites. (d) PDF fit using the $Fm\bar{3}m$ model, which allows neither Br distortion nor Cs off-centering.

Our analysis is corroborated by MD simulations of $Cs_2AgBiBr_6$ at 0.0 and 2.1 GPa (see the Supporting Information for video animations). Although the simulations were started with high-symmetry $Fm\bar{3}m$ configurations, local disorder quickly developed. The average of the MD snapshot PDFs in Figure 4a matches the $P2_1/c$ fitted PDF and experimental PDF well at both 0.0 and 2.1 GPa, including capturing the second nearest-neighbor peak. Note that these average PDFs at each pressure are computed by first calculating the PDF of each MD snapshot and then averaging those PDFs. This is distinct from first calculating the time-averaged atomic positions (as in Figure 4d and discussed below) and then calculating the PDF, as this order of operations would obscure any local-scale behavior. The short-range Br octahedral distortion and Cs off-centering in the $P2_1/c$ fitted models (Figure 4b) are in good agreement with disorder observed in the MD snapshots (Figure 4c). Despite this significant local disorder, the time-averaged MD structures (Figure 4d) match the $Fm\bar{3}m$ structures from our long-range cubic PDF fits and from XRD.[5,16] The mean squared displacements (MSDs) of atoms relative to their average MD positions are in good agreement with the thermal parameters in the XRD model and with those in the long-range $Fm\bar{3}m$ PDF fitted models (Figures S7 and S8). The Br atoms

https://dx.doi.org/10.1021/acs.jpclett.0c03412
J. Phys. Chem. Lett. 2021, 12, 532−536

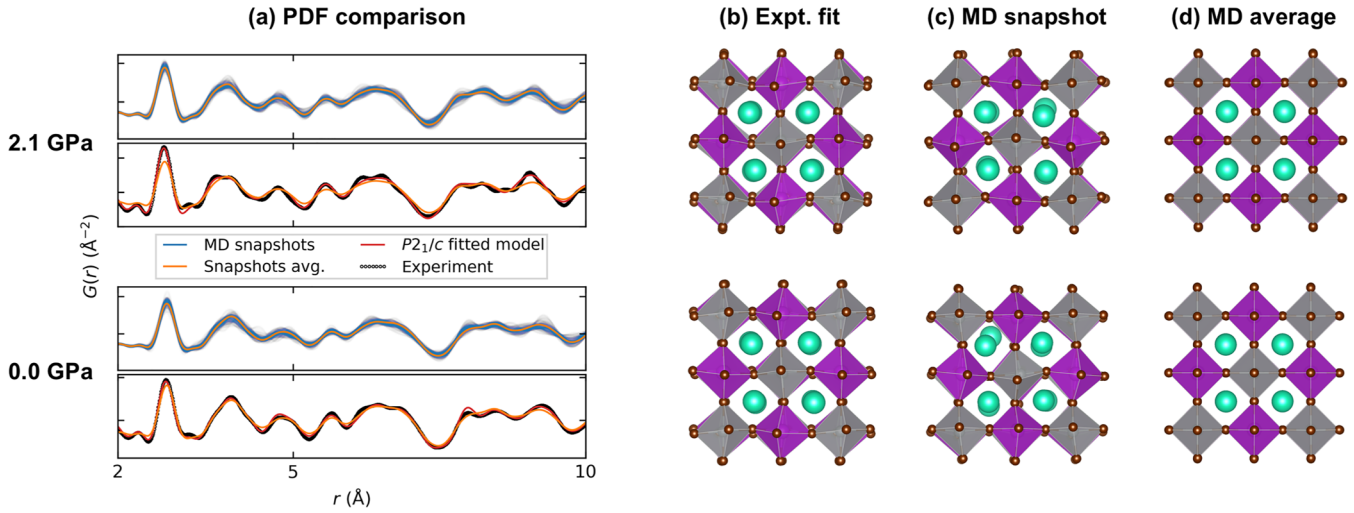

Figure 4. (a) PDFs from MD simulations and comparison with PDFs from the $P2_1/c$ fitted model and experimental data. The upper panel at each pressure shows PDFs from 1000 MD snapshots, in addition to the average of all MD snapshot PDFs. (b) Structures of the $P2_1/c$ model fitted to the experimental data at short range (2−10 Å). (c) Structures of a randomly chosen MD snapshot. (d) Time-averaged structures of MD snapshots.

consistently show larger motion perpendicular to the Bi−Br and Ag−Br bonds, and the Br MSDs from MD and PDF both become more anisotropic at 2.1 GPa relative to those at ambient pressure. As in the PDF analysis, our MD results show that local disorder of the Br atoms manifests as highly anisotropic thermal displacements when the structure is considered on average.

In summary, we have performed high-pressure X-ray total scattering on the lead-free halide double perovskite $Cs_2AgBiBr_6$. Through analysis of the X-ray and MD PDFs, we present a lower-symmetry crystallographic model which describes the local structural evolution upon compression significantly better than the cubic structure. In our model, the Br atoms are explicitly disordered, rather than having large anisotropic thermal displacements, and the Cs atoms are displaced from their high-symmetry cubic sites. These results highlight the importance of studying both the average and local structure of halide perovskites to build more accurate structure−property relationships toward obtaining desired functionality.

■ ASSOCIATED CONTENT

Supporting Information

The Supporting Information is available free of charge at https://pubs.acs.org/doi/10.1021/acs.jpclett.0c03412.

Experimental and computational details and additional figures (PDF)

(Video S1) MD animation at 0.0 GPa (MP4)

(Video S2) MD animation at 2.1 GPa (MP4)

■ AUTHOR INFORMATION

Corresponding Authors

Yu Lin − *Stanford Institute for Materials and Energy Sciences, SLAC National Accelerator Laboratory, Menlo Park, California 94025, United States;* orcid.org/0000-0001-5174-9546; Email: lyforest@stanford.edu

Wendy L. Mao − *Department of Geological Sciences, Stanford University, Stanford, California 94305, United States; Stanford Institute for Materials and Energy Sciences, SLAC National Accelerator Laboratory, Menlo Park, California 94025, United States*; Email: wmao@stanford.edu

Authors

Samuel P. Girdzis − *Department of Applied Physics, Stanford University, Stanford, California 94305, United States;* orcid.org/0000-0001-6259-9459

Linn Leppert − *Computational Chemical Physics, MESA+ Institute of Nanotechnology, University of Twente, 7500 AE Enschede, The Netherlands; Institute of Physics, University of Bayreuth, 95440 Bayreuth, Germany*

Adam H. Slavney − *Department of Chemistry, Stanford University, Stanford, California 94305, United States*

Sulgiye Park − *Department of Geological Sciences, Stanford University, Stanford, California 94305, United States;* orcid.org/0000-0001-5875-4727

Karena W. Chapman − *Department of Chemistry, Stony Brook University, Stony Brook, New York 11794, United States;* orcid.org/0000-0002-8725-5633

Hemamala I. Karunadasa − *Department of Chemistry, Stanford University, Stanford, California 94305, United States; Stanford Institute for Materials and Energy Sciences, SLAC National Accelerator Laboratory, Menlo Park, California 94025, United States;* orcid.org/0000-0003-4949-8068

Complete contact information is available at: https://pubs.acs.org/10.1021/acs.jpclett.0c03412

Notes

The authors declare no competing financial interest.

■ ACKNOWLEDGMENTS

This work was supported by the Department of Energy, Office of Science, Basic Energy Sciences, Materials Sciences and Engineering Division, under contract DE-AC02-76SF00515. L.L. acknowledges support by the Bavarian State Ministry of Science and the Arts through the Collaborative Research Network Solar Technologies Go Hybrid (SolTech), the German Research Foundation (D.F.G.) through SFB840 B7, and computational resources provided by the Bavarian Polymer Institute (BPI). This research used resources of the

Advanced Photon Source, a U.S. Department of Energy (DOE) Office of Science User Facility operated for the DOE Office of Science by Argonne National Laboratory under contract no. DE-AC02-06CH11357.

REFERENCES

(1) Green, M. A.; Ho-Baillie, A.; Snaith, H. J. The Emergence of Perovskite Solar Cells. *Nat. Photonics* **2014**, *8*, 506−514.
(2) McMeekin, D. P.; Sadoughi, G.; Rehman, W.; Eperon, G. E.; Saliba, M.; Horantner, M. T.; Haghighirad, A.; Sakai, N.; Korte, L.; Rech, B.; et al. A Mixed-Cation Lead Mixed-Halide Perovskite Absorber for Tandem Solar Cells. *Science* **2016**, *351*, 151−155.
(3) Kojima, A.; Teshima, K.; Shirai, Y.; Miyasaka, T. Organometal Halide Perovskites as Visible-Light Sensitizers for Photovoltaic Cells. *J. Am. Chem. Soc.* **2009**, *131*, 6050−6051.
(4) NREL. Best Research-Cell Efficiency Chart. https://www.nrel.gov/pv/cell-efficiency.html.
(5) Slavney, A. H.; Hu, T.; Lindenberg, A. M.; Karunadasa, H. I. A Bismuth-Halide Double Perovskite with Long Carrier Recombination Lifetime for Photovoltaic Applications. *J. Am. Chem. Soc.* **2016**, *138*, 2138−2141.
(6) McClure, E. T.; Ball, M. R.; Windl, W.; Woodward, P. M. Cs_2AgBiX_6 (X = Br, Cl): New Visible Light Absorbing, Lead-Free Halide Perovskite Semiconductors. *Chem. Mater.* **2016**, *28*, 1348−1354.
(7) Lee, Y.; Mitzi, D. B.; Barnes, P. W.; Vogt, T. Pressure-Induced Phase Transitions and Templating Effect in Three-Dimensional Organic-Inorganic Hybrid Perovskites. *Phys. Rev. B: Condens. Matter Mater. Phys.* **2003**, *68*, No. 020103.
(8) Matsuishi, K.; Ishihara, T.; Onari, S.; Chang, Y. H.; Park, C. H. Optical Properties and Structural Phase Transitions of Lead-Halide Based Inorganic-Organic 3D and 2D Perovskite Semiconductors under High Pressure. *Phys. Status Solidi B* **2004**, *241*, 3328−3333.
(9) Swainson, I. P.; Tucker, M. G.; Wilson, D. J.; Winkler, B.; Milman, V. Pressure Response of an Organic-Inorganic Perovskite: Methylammonium Lead Bromide. *Chem. Mater.* **2007**, *19*, 2401−2405.
(10) Wang, Y.; Lü, X.; Yang, W.; Wen, T.; Yang, L.; Ren, X.; Wang, L.; Lin, Z.; Zhao, Y. Pressure-Induced Phase Transformation, Reversible Amorphization, and Anomalous Visible Light Response in Organolead Bromide Perovskite. *J. Am. Chem. Soc.* **2015**, *137*, 11144−11149.
(11) Jaffe, A.; Lin, Y.; Beavers, C. M.; Voss, J.; Mao, W. L.; Karunadasa, H. I. High-Pressure Single-Crystal Structures of 3D Lead-Halide Hybrid Perovskites and Pressure Effects on Their Electronic and Optical Properties. *ACS Cent. Sci.* **2016**, *2*, 201−209.
(12) Capitani, F.; Marini, C.; Caramazza, S.; Postorino, P.; Garbarino, G.; Hanfland, M.; Pisanu, A.; Quadrelli, P.; Malavasi, L. High-Pressure Behavior of Methylammonium Lead Iodide ($MAPbI_3$) Hybrid Perovskite. *J. Appl. Phys.* **2016**, *119*, 185901.
(13) Szafrański, M.; Katrusiak, A. Mechanism of Pressure-Induced Phase Transitions, Amorphization, and Absorption-Edge Shift in Photovoltaic Methylammonium Lead Iodide. *J. Phys. Chem. Lett.* **2016**, *7*, 3458−3466.
(14) Shen, P.; Vogt, T.; Lee, Y. Pressure-Induced Enhancement of Broad-Band White Light Emission in Butylammonium Lead Bromide. *J. Phys. Chem. Lett.* **2020**, *11*, 4131−4137.
(15) Fang, Y.; Zhang, L.; Yu, Y.; Yang, X.; Wang, K.; Zou, B. Manipulating Emission Enhancement and Piezochromism in Two-Dimensional Organic-Inorganic Halide Perovskite $[(HO)(CH_2)_2NH_3)]_2PbI_4$ by High Pressure. *CCS Chem.* **2020**, 2203−2210.
(16) Li, Q.; Wang, Y.; Pan, W.; Yang, W.; Zou, B.; Tang, J.; Quan, Z. High-Pressure Band-Gap Engineering in Lead-Free $Cs_2AgBiBr_6$ Double Perovskite. *Angew. Chem., Int. Ed.* **2017**, *56*, 15969−15973.
(17) Connor, B. A.; Biega, R. I.; Leppert, L.; Karunadasa, H. I. Dimensional Reduction of the Small-Bandgap Double Perovskite $Cs_2AgTlBr_6$. *Chem. Sci.* **2020**, *11*, 7708−7715.
(18) Yang, R. X.; Skelton, J. M.; Da Silva, E. L.; Frost, J. M.; Walsh, A. Spontaneous Octahedral Tilting in the Cubic Inorganic Cesium Halide Perovskites $CsSnX_3$ and $CsPbX_3$ (X = F, Cl, Br, I). *J. Phys. Chem. Lett.* **2017**, *8*, 4720−4726.
(19) McKechnie, S.; Frost, J. M.; Pashov, D.; Azarhoosh, P.; Walsh, A.; van Schilfgaarde, M. Dynamic Symmetry Breaking and Spin Splitting in Metal Halide Perovskites. *Phys. Rev. B: Condens. Matter Mater. Phys.* **2018**, *98*, No. 085108.
(20) Steele, J. A.; Puech, P.; Keshavarz, M.; Yang, R.; Banerjee, S.; Debroye, E.; Kim, C. W.; Yuan, H.; Heo, N. H.; Vanacken, J.; et al. Giant Electron−Phonon Coupling and Deep Conduction Band Resonance in Metal Halide Double Perovskite. *ACS Nano* **2018**, *12*, 8081−8090.
(21) Fabini, D. H.; Laurita, G.; Bechtel, J. S.; Stoumpos, C. C.; Evans, H. A.; Kontos, A. G.; Raptis, Y. S.; Falaras, P.; Van der Ven, A.; Kanatzidis, M. G.; et al. Dynamic Stereochemical Activity of the Sn^{2+} Lone Pair in Perovskite $CsSnBr_3$. *J. Am. Chem. Soc.* **2016**, *138*, 11820−11832.
(22) Laurita, G.; Fabini, D. H.; Stoumpos, C. C.; Kanatzidis, M. G.; Seshadri, R. Chemical Tuning of Dynamic Cation Off-Centering in the Cubic Phases of Hybrid Tin and Lead Halide Perovskites. *Chem. Sci.* **2017**, *8*, 5628−5635.
(23) Maughan, A. E.; Ganose, A. M.; Candia, A. M.; Granger, J. T.; Scanlon, D. O.; Neilson, J. R. Anharmonicity and Octahedral Tilting in Hybrid Vacancy-Ordered Double Perovskites. *Chem. Mater.* **2018**, *30*, 472−483.
(24) Maughan, A. E.; Paecklar, A. A.; Neilson, J. R. Bond Valences and Anharmonicity in Vacancy-Ordered Double Perovskite Halides. *J. Mater. Chem. C* **2018**, *6*, 12095−12104.
(25) Bechtel, J. S.; Van der Ven, A. Octahedral Tilting Instabilities in Inorganic Halide Perovskites. *Phys. Rev. Mater.* **2018**, *2*, No. 025401.
(26) Bechtel, J. S.; Thomas, J. C.; Van der Ven, A. Finite-Temperature Simulation of Anharmonicity and Octahedral Tilting Transitions in Halide Perovskites. *Phys. Rev. Mater.* **2019**, *3*, 113605.
(27) Hammersley, A. P. FIT2D: A Multi-Purpose Data Reduction, Analysis and Visualization Program. *J. Appl. Crystallogr.* **2016**, *49*, 646−652.
(28) Qiu, X.; Thompson, J. W.; Billinge, S. J. L. PDFgetX2: A GUI-Driven Program to Obtain the Pair Distribution Function from X-Ray Powder Diffraction Data. *J. Appl. Crystallogr.* **2004**, *37*, 678.
(29) Farrow, C. L.; Juhas, P.; Liu, J. W.; Bryndin, D.; Božin, E. S.; Bloch, J.; Proffen, T.; Billinge, S. J. L. PDFfit2 and PDFgui: Computer Programs for Studying Nanostructure in Crystals. *J. Phys.: Condens. Matter* **2007**, *19*, 335219.
(30) Kresse, G.; Hafner, J. Norm-Conserving and Ultrasoft Pseudopotentials for First-Row and Transition Elements. *J. Phys.: Condens. Matter* **1994**, *6*, 8245−8257.
(31) Kresse, G.; Furthmüller, J. Efficient Iterative Schemes for Ab Initio Total-Energy Calculations Using a Plane-Wave Basis Set. *Phys. Rev. B: Condens. Matter Mater. Phys.* **1996**, *54*, 11169−11186.
(32) Csonka, G. I.; Perdew, J. P.; Ruzsinszky, A.; Philipsen, P. H. T.; Lebègue, S.; Paier, J.; Vydrov, O. A.; Ángyán, J. G. Assessing the Performance of Recent Density Functionals for Bulk Solids. *Phys. Rev. B: Condens. Matter Mater. Phys.* **2009**, *79*, 1−14.
(33) Momma, K.; Izumi, F. VESTA 3 for Three-Dimensional Visualization of Crystal, Volumetric and Morphology Data. *J. Appl. Crystallogr.* **2011**, *44*, 1272−1276.
(34) Glazer, A. M. The Classification of Tilted Octahedra in Perovskites. *Acta Crystallogr., Sect. B: Struct. Crystallogr. Cryst. Chem.* **1972**, *28*, 3384−3392.
(35) Howard, C. J.; Kennedy, B. J.; Woodward, P. M. Ordered Double Perovskites − a Group-Theoretical Analysis. *Acta Crystallogr., Sect. B: Struct. Sci.* **2003**, *59*, 463−471.

https://dx.doi.org/10.1021/acs.jpclett.0c03412
J. Phys. Chem. Lett. 2021, 12, 532−536